FAILURE ASSESSMENT OF CAST STEEL BRIDGE PIERS BY THE CEGB R6-CONCEPT OF FRACTURE MECHANICS

H. AMSTUTZ[1], W. DAHL[2], P. LANGENBERG[2], and T. SEEGER[1]

[1] *Fachgebiet Werkstoffmechanik, Technische Hochschule Darmstadt, D-64287 Darmstadt, Germany*

[2] *Institut für Eisenhüttenkunde, Rheinisch-Westfälische Technische Hochschule Aachen, D-52056 Aachen, Germany*

ABSTRACT

The quantification of the strength of cast steel is often difficult because of unavoidable inhomogenities ranging from pores or spongy structure up to crack-like defects. To get a lower limit of the strength, the defects which would be covered by the German guidelines for cast steel components on non-destructive testing were interpreted as cracks and assessed by the CEGB R6-Procedure of fracture mechanics. The results show that the toughness of the material considered is sufficient to reach the yield stress and even higher levels near the ultimate stress.

KEYWORDS

Fracture mechanical assessment, R6-concept, J-integral-concept, strength of cracked structures, cast steel.

INTRODUCTION

A lot of buildings are being erected at present in Berlin in the future government quarter. Among these is the new "Kronprinzen"-Bridge over the river Spree. The design is a modern, very light construction, Fig. 1, but because of some postulated structural features the piers could not be constructed in the usual way by welding of rolled steel profiles and plates. The only alternative was to cast the piers as a whole, Fig. 2, using a cast steel denoted as GS-13MnNi 6 4 with the chemical analysis and the mechanical properties listed in Tables 1 and 2.

In assessing the strength of the cast steel the question arises as to how the unavoidable inhomogenities in the form of pores or spongy structure and possibly crack-like defects ought to be considered. The answer has to be oriented to the maximum defects allowed by the German code DIN 1690 as being detected by ultra-sonic or x-ray non-destructive testing. The application of DIN 1690 leads to the worst case defect pattern of Fig. 3 a which although rather improbable must be assumed because it would be covered by the quality standards postulated. Finally, the generally voluminous but indefinite shape of the defects were considered as elliptical cracks in the plane of the cross-section.

THE REDUCTION OF THE BEARING CROSS-SECTION BY THE DEFECTS

The conventional proof strength of a component is based on

$$\sigma_{perm} = \frac{N}{A} + \frac{M}{W} \leq \frac{\sigma_Y}{\gamma} \tag{1}$$

where σ_{perm} is the permissable maximum stress, N and M the axial and bending load, A and W are the area and the section modulus of the cross-section, σ_Y is the yield stress of the material and γ the relevant safety factor. To keep the proof stresses defined by relating the forces and moments to the uncracked gross section also for the defective cross-section, the loss of area by the many cracks is taken into account by a formal reduction of the yield stress. If the centroid of the gross and the net sections essentially coincide as would be true for the regular crack pattern, the reduction is equal to the ratio of the net section to the gross section, so that in axial loading

$$\frac{\sigma_{Y,red}}{\sigma_Y} = \frac{A_{net}}{A_{gr}} \tag{2}$$

Besides the regular crack distribution a more unfavourable arrangement cannot be ruled out. To include this worst case various non-regular crack distributions were considered yielding the most unfavourable crack pattern for axial loading, shown in Fig. 3 b. The difference between the centroid of gross and net sections results in a superposed bending moment leading to

$$\frac{\sigma_{Y,red}}{\sigma_Y} = \frac{\frac{N}{A_{gr}}}{\frac{N}{A_{net}} + \frac{N \cdot \Delta y_s}{W_{net}}} = \frac{\frac{1}{A_{gr}}}{\frac{1}{A_{net}} + \frac{\Delta y_s}{W_{net}}} \tag{3}$$

where Δy_s is the vertical difference of the centroids. Though containing less cracks, the non-regular distribution gives higher edge stresses and a lower reduction factor. In bending, the reduction is given by

$$\frac{\sigma_{Y,red}}{\sigma_Y} = \frac{W_{net}}{W_{gr}} \tag{4}$$

where the regular crack arrangement yields the worst result.

Numerical calculations were carried out by dividing the cross-section into 100 horizontal layers of constant thickness Δy and subtracting the parts of the elliptical cracks. The reduction factors $\sigma_{Y,red}/\sigma_Y$ obtained were 0.845 or 0.801, respectively for axial loading and 0.861 for bending. For simplicity, all subsequent computations are based on a factor of 0.80.

Now Eqn (1) reads more precisely

$$\sigma_{perm} = \frac{N}{A_{gr}} + \frac{M}{W_{gr}} = \sigma_{N,gr} + \sigma_{B,gr} \leq \frac{\sigma_{Y,red}}{\gamma} \tag{5}$$

with $\sigma_{N,gr}$ and $\sigma_{B,gr}$ as the relevant load quantities.

THE ASSESSMENT OF THE DEFECTIVE STEEL PIERS BY THE R6-PROCEDURE

The CEGB R6-procedure for the assessment of cracked structures (Milne *et. al.*, 1988) constitutes a specialisation of the J-integral-concept in fracture mechanics. The fracture

condition

$$J = J_c \tag{6}$$

is represented by a curve K_r versus L_r in the Failure Assessment Diagram (FAD), Fig. 6. The quantity K_r describes the normalized local load intensity K_I/K_{mat} where K_I is the Stress Intensity Factor (SIF) of elasticity and K_{mat} the corrresponding value of material toughness. The quantity L_r denotes the global load level $\sigma_{N,gr}$ or $\sigma_{B,gr}$ related to the corresponding plastic limit load (PLL) $\sigma_{gr,Y}$. The load range is limited to $L_r = \sigma_u/\sigma_Y$ by the "cut off" line. The limit curve divides the range of local and global states into a safe region below and left of the curve and an unsafe region above and right of the curve.

There are three "Options" for the assessment depending on the input data available and the effort that one is willing to invest. We chose Option 2 which is based on the individual "true" stress-strain curve $\varepsilon_{true} = f(\sigma_{true})$ of the material concerned. The limit curve is given by

$$K_r = \left(\frac{E\varepsilon_{ref}}{L_r\sigma_Y} + \frac{L_r^3\sigma_Y}{2E\varepsilon_{ref}}\right)^{-1/2} \tag{7}$$

where ε_{ref} follows from the σ-ε-curve after substituting $\sigma = L_r\sigma_Y$

$$\varepsilon_{ref} = f(\sigma_{ref}) = f(L_r\sigma_Y) \tag{8}$$

On the basis of the limit curve of the FAD, various aspects of the assessment can be considered, for example the demanded toughness, the acceptable crack size or load, or the remaining safety. In the present case, the main reason of the assessment was the quantification of safety against fracture for given crack size, load, and toughness of the material. This requires the determination of the SIF, the PLL of the structure, and the relevant K_{mat}-values of the material as K_{Ic} or K_c or as derived from critical J-value according to $K_{mat} = \sqrt{EJ/(1-\nu^2)}$.

Determination of SIF. The handbook of Murakami *et al.* (1987) offers a solution for two neighbouring elliptical cracks in an infinite body under tension. The influence of finite width increases this SIF by a factor of 1.03, resulting in

$$\frac{K_I}{\sigma_{N,gr}} = 4.9 \text{ mm}^{1/2} \tag{9}$$

for axial loading and

$$\frac{K_I}{\sigma_{B,gr}} \approx 4.5 \text{ mm}^{1/2} \tag{10}$$

in the case of bending. The non-regular crack pattern has not been further considered as it is less unfavourable than the regular distribution.

Calculation of the plastic limit load. The plastic limit loads in axial and bending loading are

$$\sigma_{N,gr,Y} = \frac{N_{net,Y}}{A_{gr}} \tag{11}$$

and

$$\sigma_{B,gr,Y} = \frac{M_{net,Y}}{W_{gr}} \tag{12}$$

Applying the mentioned layer model of the cross section, we obtain $N_{net,Y}$ as

$$N_{net,Y} = \sum_{i=1}^{100} \sigma\, x_i \Delta y - \sum_{i=1}^{54} \sigma\, A_{ell} \tag{13}$$

where x_i denotes the variable layer width and A_{ell} the area of the elliptical cracks. The stress σ stands for $+\sigma_Y$ in the section with positive stress and for $-\sigma_Y$ in the section with negative stress, Fig. 4 a. The line $y = y_o$ separating the sections has to be determined iteratively, so that the resulting bending moment with respect to the centroid of the uncracked cross-section becomes zero

$$M = \sum_{i=1}^{100} \sigma\, x_i y_i \Delta y - \sum_{i=1}^{54} \sigma\, y_{s,i} A_{ell} = 0 \tag{14}$$

The PLL in bending, Fig. 4 b, is given as

$$M_{net,Y} = \sum_{i=1}^{100} \sigma\, x_i y_i \Delta y - \sum_{i=1}^{54} \sigma\, y_{s,i} A_{ell} \tag{15}$$

satisfying the condition

$$N = \sum_{i=1}^{100} \sigma\, x_i \Delta y - \sum_{i=1}^{54} \sigma\, A_{ell} = 0 \tag{16}$$

In Eqns (14) and (15) y_i and $y_{s,i}$ signify the y-coordinate of the centroids of the layer and the elliptical cracks.

The computation of the PLL results in $\sigma_{N,gr,Y} = 0.842 \cdot \sigma_Y$ and $\sigma_{B,gr,Y} = 1.465 \cdot \sigma_Y$.

Fracture toughness. By a number of 20% side-grooved standard-C(T)-specimen (W = 100 mm, B = 50 mm, a/W = 0.5) the dependence of the K_{Ic}- or J_{Ic}-values, respectively on temperature was investigated showing a transition region around –20°C. Further experiments with C(T)-specimen with and without side-grooves and large M(T)-specimen (center cracked plates W = 200 mm, B = 60 mm, a/W = 0.1) were carried out to establish the valid toughness values for +20°C and the lower service temperature –30°C, see Fig. 5.

The tests yielded the lowest J_c of 67 N/mm at –30° equivalent to K_{mat} = 3930 N/mm$^{3/2}$. The C(T)-specimen without side-grooves which seem to reproduce the local states more realistically lead to J_i-values around 400 N/mm equal to K_{mat} = 9600 N/mm$^{3/2}$ showing a well-developed stretch zone at –30°C. At the same temperature, the low constraint M(T)-specimen reached a J_i-value near 800 N/mm equal to K_{mat} = 13590 N/mm$^{3/2}$ after considerable ductile deformations.

Discussion of the FAD results. An important information from the FAD is the minimum necessary toughness for reaching the PLL to avoid brittle fracture (dashed line ① in Fig. 6 and Fig. 7).

For steels with a distinct yield point the limit curve of Option 2 reduces within $0 < L_r \leq 1$ to

$$K_r = (1 + 0.5 L_r^2)^{-1/2} \tag{17}$$

because $\varepsilon_{ref} = L_r \sigma_Y / E$ in this range. On the level of the PLL i.e. $L_r = 1$ Eqn (17) gives $K_r = 0.82 = K_I / K_{mat}$. To ensure this state a K_{mat}-value of $K_I/0.82$ is demanded.

With $K_I = 4.9\, \sigma_{N,gr,Y}$ for axial loading and $K_I = 4.5\, \sigma_{B,gr,Y}$ for bending the postulated K_{mat}-values are 1786 N/mm$^{3/2}$ or 2854 N/mm$^{3/2}$, respectively. Since the lowest K_{mat} for –30°C amounts to 3930 N/mm$^{3/2}$ the attainment of the PLL should be guaranteed.

A second aspect of safety is the reliable development of larger plastic deformations. For axial loading, already on the basis of the lowest K_{mat} for side-grooved C(T)-specimen extensive yielding on the level of PLL can be expected (Fig. 6, solid line ②). This holds also for bending with respect to the higher stretched zones of the cross section, Fig. 7.

While in the case of axial loading IT IS understandable that no significant increase of safety margins between the stress $\gamma\, \sigma_{perm}$ and $\sigma_{N,gr,Y}$ can be expected, the potential of bending between first yielding of the extreme fibers and the fully plastic state results in an additional safety factor of 1.8.

The higher toughness values of non-side-grooved C(T)- and M(T)-specimens lift the critical states of the net section axial loading up to the level of the ultimate stress (solid lines ③ and ④ in Fig. 6 and Fig.7). The relatively higher local loading of the outer fibers from bending causes fracture states below the cut off and especially for the K_{mat} of M(T)-specimen distinctly above the PLL in the hardening range.

REFERENCES

Milne, I., Ainsworth, R. A., Dowling, A. R. and Stewart, A. T. (1988). Assessment of the Integrity of Structures Containing Defects. *Int. J. Pressure Vessels & Piping*, 32, 3-104.

Murakami, Y. (1987). *Stress Intensity Factors Handbook.* Joint Publication by the Society of Materials Sciences, Japan and Pergamon Press, Kyoto

C	Si	Mn	P	S	Cr	Ni	Mo
0.101	0.426	1.142	0.019	0.0069	0.047	0.892	0.139
Zr	V	Al	Cu	Nb	Ti	O	N
0.0052	0.0016	0.036	0.026	0.0002	0.0010	0.0037	0.0089

Table 1 Chemical analysis of cast steel GS-13MnNi 6 4 in % (means)

σ_Y yield stress [N/mm^2]	$\sigma_{Y,red}$ yield stress reduced [N/mm^2]	σ_u ultimate stress [N/mm^2]	E Young's modulus [N/mm^2]	ν Poisson's ratio [–]
355	284	480	210000	0.3

Table 2 Mechanical properties

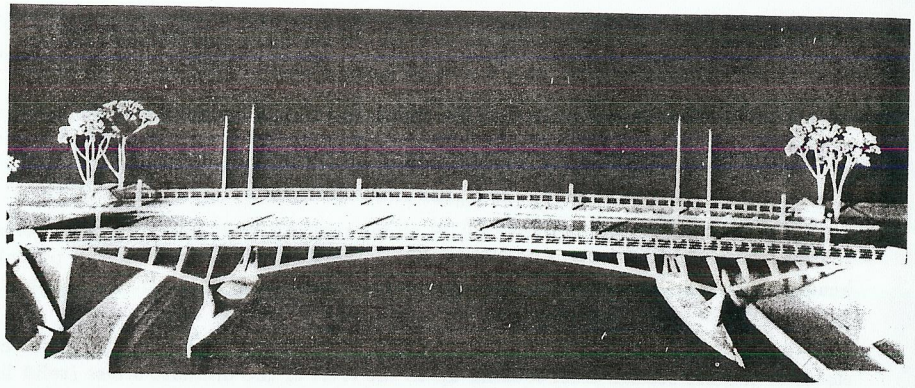

Fig. 1 The new "Kronprinzen"-bridge in Berlin (design of architect Calatrava)

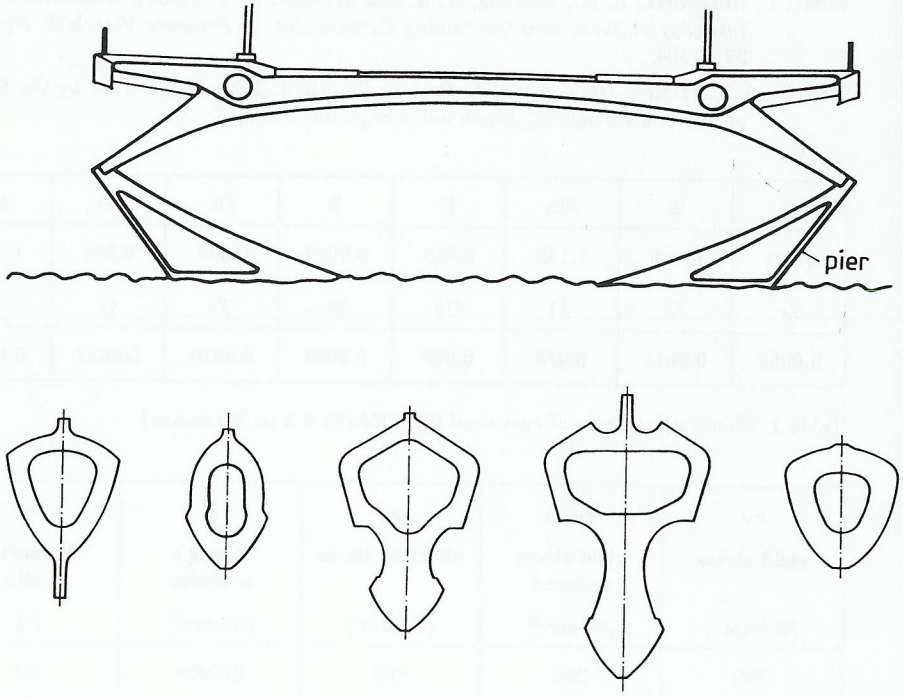

Fig. 2 Transverse section of the bridge with various cross-sections of the casted piers

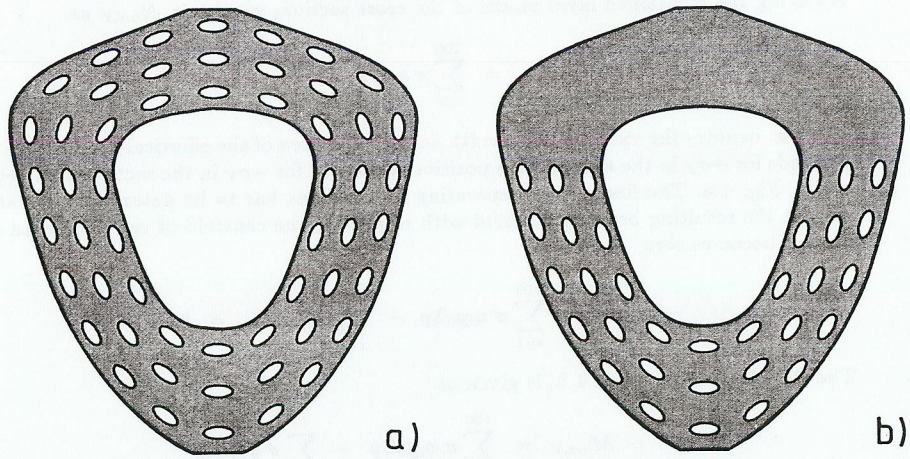

Fig. 3 Investigated cross-section with regular and non-regular crack distribution

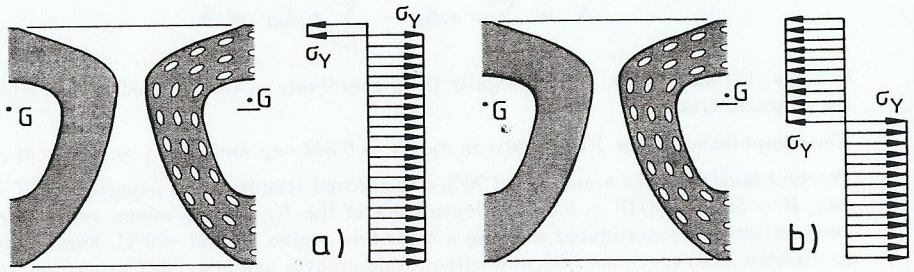

Fig. 4 Fully plastic stress distribution for axial loading a) and bending b)

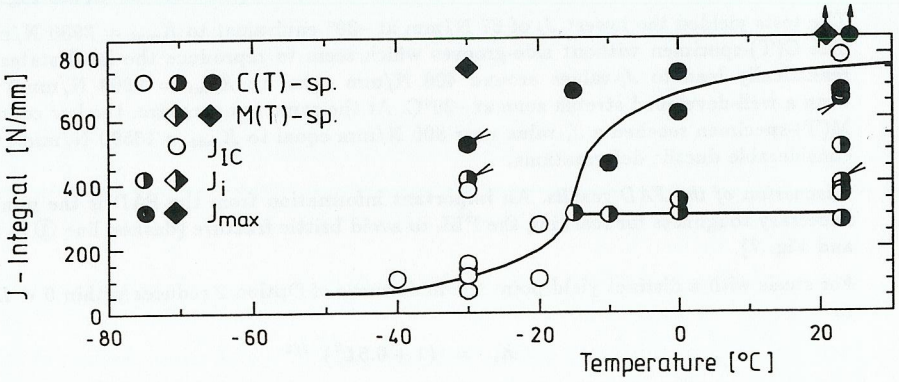

Fig. 5 Fracture mechanics test results of GS-13MnNi 6 4 (○◑● non-side-grooved)

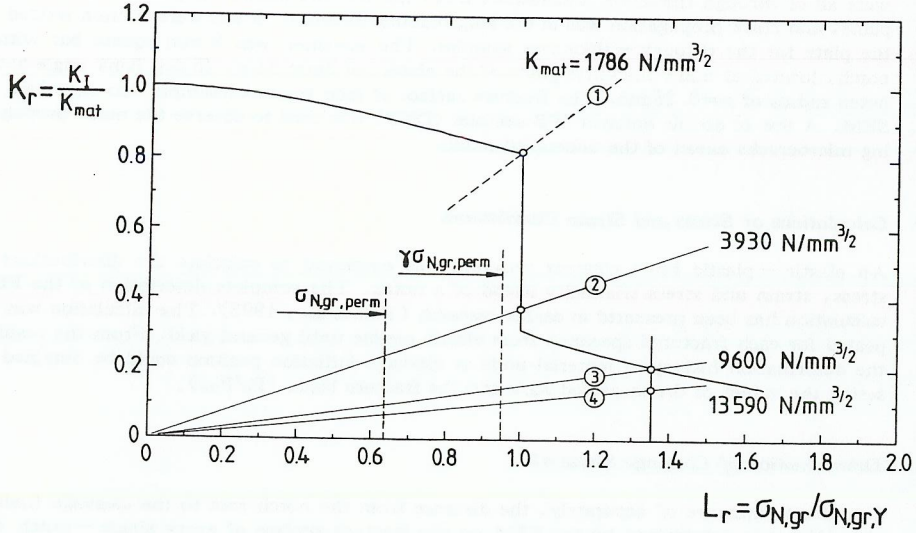

Fig. 6 R6-FAD Option 2 cast steel GS-12MnNi 6 4, axial loading

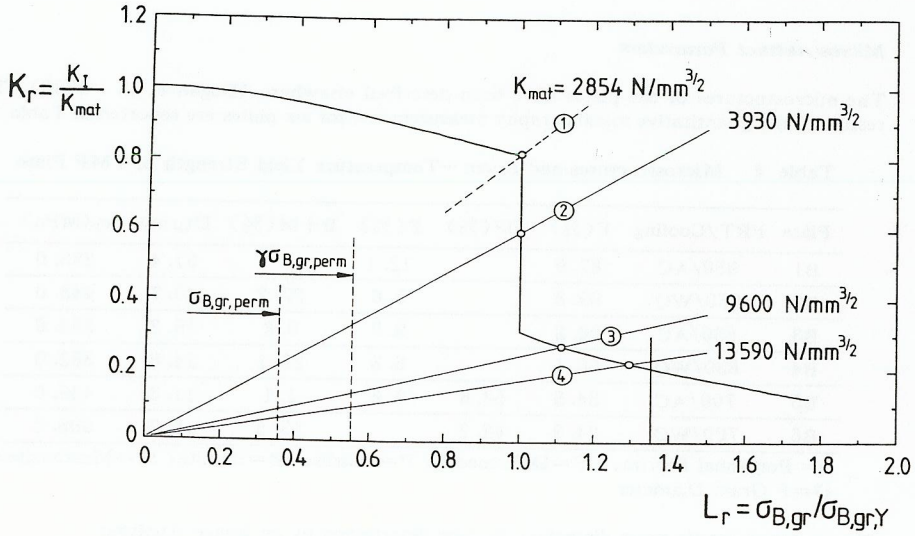

Fig. 7 R6-FAD Option 2 cast steel GS-13MnNi 6 4, bending